Abdominal Radiology

© Springer Science+Business Media New York 2016
Published online: 17 June 2016

Abdom Radiol (2016) 41:2102–2114
DOI: 10.1007/s00261-016-0811-y

MR comparative study of combined hepatocellular-cholangiocarcinoma in normal, fibrotic, and cirrhotic livers

Ruo Fan Sheng,[1,2] Yan Hong Xie,[3] Yuan Ji,[3] Cai Zhong Chen,[1,2] Li Yang,[1,2] Kai Pu Jin,[1,2] Meng Su Zeng[1,2]

[1]Department of Radiology, Zhongshan Hospital, Fudan University, No. 180 Fenglin Road, Xuhui District, Shanghai 200032, China
[2]Shanghai Institute of Medical Imaging, No. 180 Fenglin Road, Xuhui District, Shanghai 200032, China
[3]Department of Pathology, Zhongshan Hospital, Fudan University, No. 180 Fenglin Road, Xuhui District, Shanghai 200032, China

Abstract

Purpose: To compare MR imaging features of combined hepatocellular-cholangiocarcinoma (cHCC-CC) in normal, fibrotic, and cirrhotic livers.
Methods: A total of 64 patients with 67 pathologically proven cHCC-CCs were retrospectively analyzed. Patients were classified into three groups according to the patients' liver condition: patients with normal liver (F0, group 1), fibrosis without cirrhosis (F1–3, group 2), and cirrhosis (F4, group 3). The morphological and MR signal features on T1- and T2-weighted, dynamic contrast-enhanced, diffusion-weighted imaging, as well as the accompanying imaging findings, were evaluated and compared.
Results: There were 12, 19, and 33 patients in groups 1, 2, and 3, respectively. Tumors in the fibrotic and cirrhotic livers were smaller than those in the normal liver, and tumors with cirrhosis had the smallest size ($P = 0.0326$). No statistical difference was found when comparing the signal intensity on T2-weighted imaging ($P = 0.496$), but iso- or hypointense lesions were only found in the fibrosis ($n = 2$) or cirrhosis group ($n = 2$). Enhancement pattern was different between groups, the washout pattern was more often seen in the cirrhosis group ($P = 0.049$), and the accompanying mosaic architecture was also more commonly seen in the cirrhosis group ($P = 0.048$). The ADC values of the lesions were not different among the three groups ($P = 0.899$).
Conclusion: MRI may provide valuable information for the diagnosis and differential diagnosis of cHCC-CC in normal, fibrotic, and cirrhotic livers. The nodule size, enhancement pattern, and the presence of mosaic architecture in cHCC-CC differ between different degrees of background liver disease.

Key words: Combined hepatocellular-cholangiocarcinoma—Magnetic resonance imaging—Cirrhosis—Fibrosis

Combined hepatocellular-cholangiocarcinoma (cHCC-CC) is a rare variant of primary liver cancers (ranging from 0.4 % to 14.2 %), comprising elements of both hepatocellular carcinoma (HCC) and cholangiocarcinoma (CC), which are intimately admixed [1, 2], with prognosis poorer than or intermediate between the two [3–8]. Clinical features including abdominal pain, malaise, palpable mass, fever, and jaundice of cHCC-CC have been reported in several studies, but they are unspecific and overlap with both HCC and CC [6, 9].

MR findings of cHCC-CC are still not conclusive nowadays and are frequently similar to HCC and CC, so these tumors are difficult to prospectively diagnose [10]. It is widely recognized that chronic hepatitis and the evolving cirrhosis are the main risk factors for HCC and CC, but in the recent years cHCC-CC has been increasingly found in these specific backgrounds, especially in Asia [11]. The chronic liver disease background makes diagnosis more difficult as tumor characterization may be hampered by the distortion of the hepatic parenchyma and liver inhomogeneity due to the fibrotic process [12, 13]. de Campos et al. [14] observed a correlation between the presence of cirrhosis and the observed enhancement pattern, while Wells et al. [13] found

Correspondence to: Meng Su Zeng; *email:* mengsuzeng@163.com

no correlations. In addition, the presence of fibrosis/cirrhosis may be one of the most important predictors of death as the decompensated microenvironment would increase the risk of surgery and mortality [15]. Thus, we aimed to compare MR imaging features of cHCC-CC in normal, fibrotic, and cirrhotic livers to identify whether background liver disease was associated with imaging patterns of cHCC-CC.

Materials and methods

Patients

This retrospective study was approved by the institutional review board and informed consent was waived. Patients were retrospectively identified, and the pathologic diagnosis was confirmed by a pathologist (Y.H.X. with 8 years of experience in liver pathology) by searching our institution's pathology database between January 2010 and June 2015. The inclusion criteria were (a) pathologically proven cHCC-CC, (b) abdominal contrast-enhanced MRI performed in our institution with satisfactory image quality following standard protocol within 10 days prior to hepatectomy, and (c) no history of prior oncologic treatment or liver resection.

A total of 67 cHCC-CC cases were picked out according to the inclusion criteria, but 3 of them were excluded due to poor MR quality. Finally, 64 patients (52 men and 12 women; mean age: 53.4 years) were included. The histopathologic diagnosis of cHCC-CC was confirmed by surgical resection ($n = 61$) or orthotopic liver transplantation ($n = 3$).

Image acquisition

MRI was performed using a 1.5-Tesla scanner (Avanto; Siemens, Erlangen, Germany) with a peak gradient amplitude of 45 mT/m. The conventional MR protocol used in this study included transverse respiratory-navigated T2-weighted fat-suppressed turbo spin-echo sequence (TR/TE = 3500/84 ms; section thickness: 5 mm; intersection gap: 1 mm; 168 × 320 matrix) and transverse T1-weighted in-phase and opposed-phase gradient echo (TR/TE = 6.8/2.35 (in-phase), 4.75 (opposed-phase) ms; section thickness: 5 mm; intersection gap: 1 mm; 180 × 320 matrix). Diffusion-weighted imaging (DWI) was required with a transverse single-shot spin-echo echo-planar sequence (TR/TE = 2400/66 ms; section thickness: 5 mm; intersection gap: 1 mm; 168 × 320 matrix) with two *b* values (0 and 500 s/mm^2). Dynamic imaging was performed with transverse and coronal breath-hold T1-weighted 3-dimensional volumetric interpolated body examination sequence (TR/TE = 5.0/2.3 ms; section thickness: 5 mm; no intersection gap; 270 × 360 matrix) following the intravenous administration of gadopentetate dimeglumine (Magnevist; Bayer HealthCare, Berlin, Germany). Gadopentetate dimeglumine was administered at a dose of 0.1 mmol/kg at a rate of 2 mL/s, followed by a 20-mL saline flush using a power injector (Spectris; Medrad, Pittsburgh, PA). The arterial phase acquisition was triggered automatically when contrast media reached the ascending aorta. For subsequent acquisition, dynamic T1-weighted MRI at 60 s (the portal venous phase) and 180 s (the delay phase) was performed. The field of view was optimized to the patients' body habitus at 285 × 214–308 × 380 mm.

Image analysis

All images were evaluated using a picture archiving and communication system (PACS; Pathspeed, GE Medical Systems Integrated Imaging Solutions, Prospect, IL, USA). MR findings were retrospectively and independently analyzed by two abdominal radiologists (M.S.Z. and L.Y. with, respectively, 30 and 10 years of experience in abdominal imaging) in a blinded manner. The reviewers knew that the patients had liver tumors but were unaware of all other information regarding patients' history, laboratory, and final pathological results. The MR images of individual cases of cHCC-CC were presented randomly to create the setting of clinical practice to avoid bias. In three subjects in which more than one tumor mass was evaluated, no dominant mass was present and tumor masses located in separate segments were evaluated. The MR images were compared one by one according to the lesion size and location so as to ensure that the nodule analyzed was the same as that resected.

Qualitative analysis

For the morphological features, the observers measured the tumor size (maximal diameter), number (single/multiple), contour (round/lobulated/irregular), location (left/right/caudate lobe/bilobar), and distribution (subcapsular/paravascular distributed or not). Paravascular distribution means the tumor located near major hepatic vessels.

Signals on T2-weighted images were defined as (a) homogenously hyperintense, (b) heterogeneously hyperintense, (c) peripherally hyperintense, (d) centrally hyperintense, and (e) iso- or hypointense. Signals on arterial phase were registered as (a) globally hyperintense, (b) heterogeneously hyperintense, (c) peripherally hyperintense, and (d) iso- or hypointense. Dynamic enhancement patterns were defined as (a) the HCC-like pattern: contrast uptake during arterial phase followed by contrast washout which showed relative hypointensity on portal or delayed phases; (b) the CC-like pattern: peripheral or partial hyperenhancement during arterial phase followed by centripetally progressive or persistent

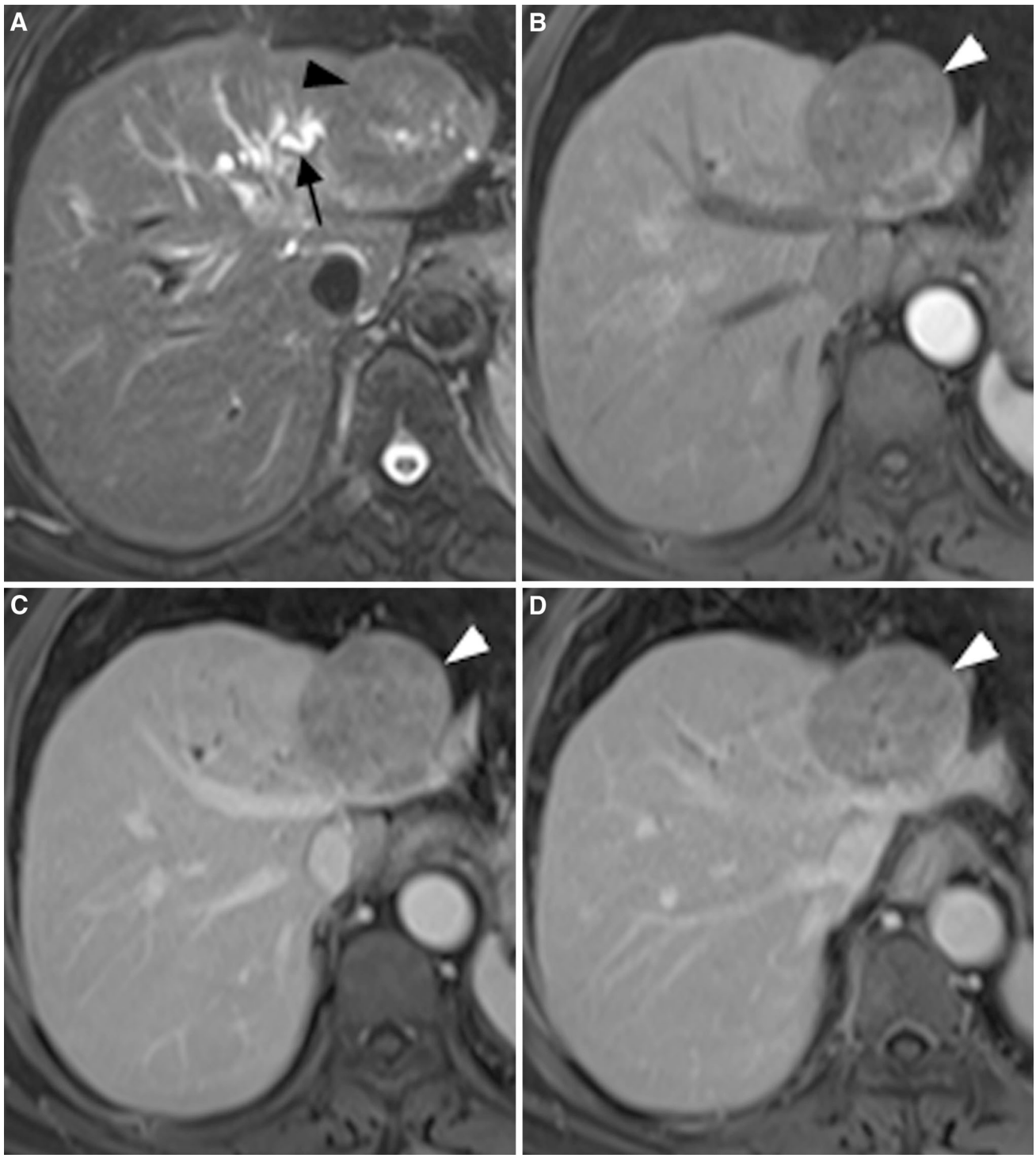

Fig. 1. Combined hepatocellular-cholangiocarcinoma in a 70-year-old man with cirrhosis (F4). **A** Transverse T2-weighted image shows a hypointense tumor (*black arrowhead*). Transverse T1-weighted VIBE images show persistent hypointensity during **B** arterial, **C** portal, and **D** delayed phases after contrast. Note the accompanying **E**, **F** bile duct invasion with cancer embolus (*white arrows*), intrahepatic bile duct dilation (*black arrow* in **A**), and hepatic capsule bulging (*white arrowheads*). Microscopy shows **G** the CC component with abundant fibrous stroma (hematoxylin–eosin stain, ×50) and **H** the HCC component with cholestasis (hematoxylin–eosin stain, ×100).

enhancement on portal or delayed phases; (c) the mixed pattern: a mix of both patterns; and (d) persistently global hyperenhancement.

Accompanying findings including the presence of satellite nodules, delayed capsule-like enhancement, mosaic architecture, hepatic capsule retraction/bulging,

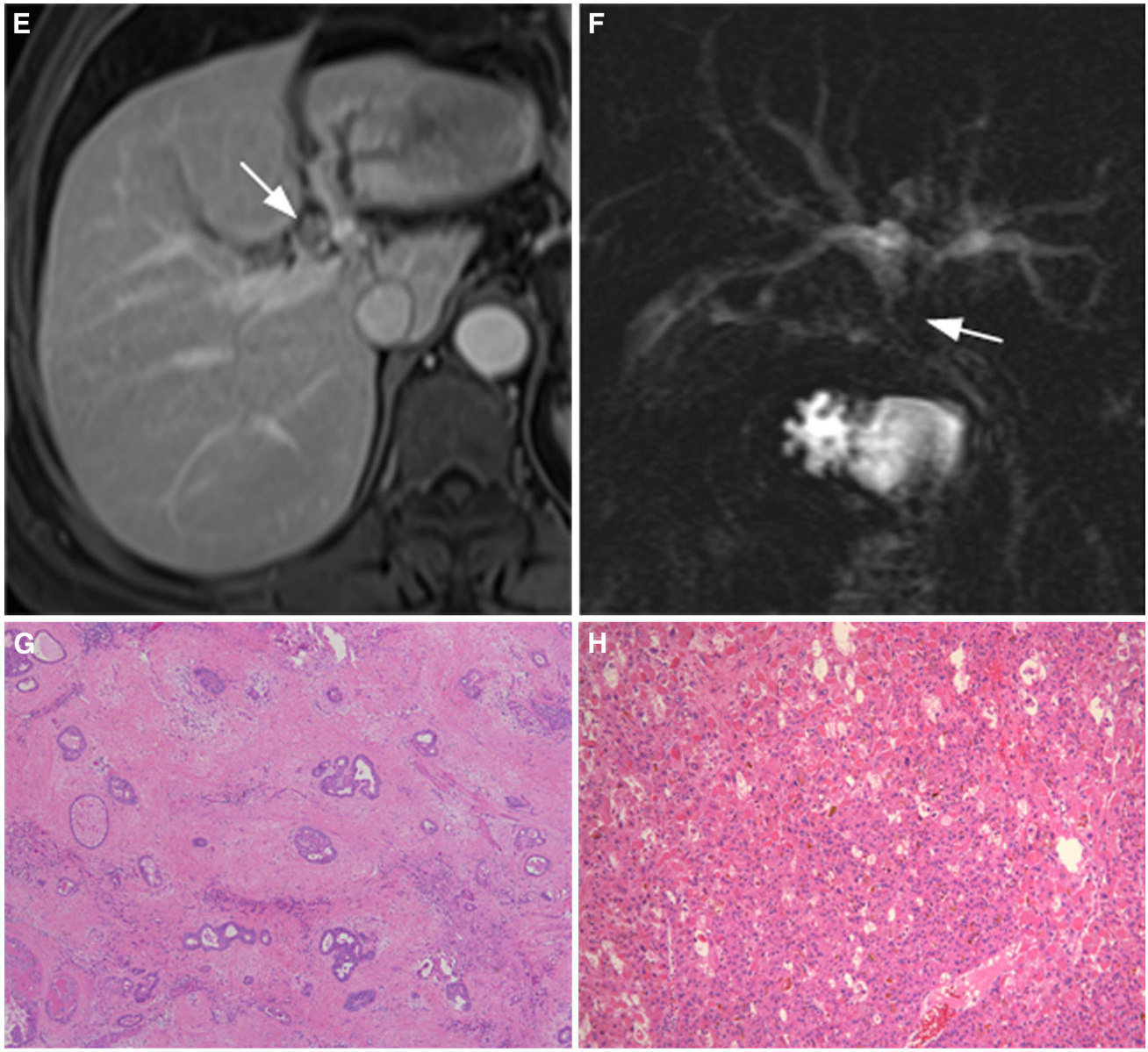

Fig. 1. continued.

bile duct dilation, transient hepatic intensity difference (THID), necrosis, hemorrhage, vascular invasion, cancer embolus, bile duct invasion, positive lymph node (imaging criteria of extrahepatic nodular lesion along the expected location of the lymphatic chain, with minimum diameter ≥10 mm or central necrosis), and distant metastasis were also analyzed. Delayed capsule-like enhancement was defined as a thin rim-like enhancement along the periphery of the lesion during the portal or delayed phases. Mosaic architecture was defined as separated enhancement in the center of the lesion during dynamic enhancement.

Quantitative analysis

Regarding the measurement of the apparent diffusion coefficient (ADC) values, ROI was manually drawn on the diffusion-weighted images, including the whole lesion, and great care was taken to avoid large vessels, necrosis, hemorrhage, and artifacts; these ROIs were then copied onto the ADC maps, and the ADC values were assessed. Two measurements were taken for each ROI by one radiologist (R.F.S. with 6 years of experience in abdominal imaging), and the average was used for analysis.

Table 1. Main tumor MR characteristics ($n = 67$)

Variable	Group 1 ($n = 13$)	Group 2 ($n = 20$)	Group 3 ($n = 34$)	P
Signal on T2-weighted images				0.496
Homogenously hyper	1	3	10	
Heterogeneously hyper	10	9	17	
Peripherally hyper	2	5	4	
Centrally hyper	0	1	1	
Iso or hypo	0	2	2	
Signal on arterial phase				0.191
Globally hyper	4	0	5	
Heterogeneously hyper	7	14	21	
Peripherally hyper	2	6	7	
Iso or hypo	0	0	1	
Dynamic enhancement pattern				0.049*
HCC-like	3	1	14	
CC-like	6	12	12	
Mixed	3	7	6	
Persistently global hyper	1	0	2	
Accompanying findings Y/N				
Satellite nodules	2/11	1/19	10/24	0.076
Capsule-like enhancement	10/3	11/9	24/10	0.425
Mosaic architecture	4/9	4/16	18/16	0.048*
Hepatic capsule retraction	0/13	3/17	5/29	0.374
Hepatic capsule bulging	4/9	5/15	10/24	1.000
Bile duct dilation	7/6	12/8	14/20	0.418
THID	4/9	8/12	13/21	0.892
Necrosis	7/6	15/5	15/19	0.082
Hemorrhage	4/9	4/16	5/29	0.431
Vascular invasion	2/11	6/14	5/29	0.393
Cancer embolus	0/13	1/19	2/32	1.000
Bile duct invasion	0/13	2/18	3/31	0.695
Positive lymph node	2/11	3/17	4/30	1.000
Distant metastasis	2/11	4/16	4/30	0.739
ADC ($\times 10^{-3}$mm^2/s)[a]	1.05(0.95,1.29)	1.10(0.91,1.43)	1.15(0.95,1.30)	0.899

Unless otherwise specified, data are numbers of lesions; hyper/iso/hypo, hyperintense/isointense/hypointense relative to the liver parenchyma
THID transient hepatic intensity difference
* $P < 0.05$
[a] Data are median, with interquartile range in parentheses

Pathological analysis

The specimens were initially evaluated by the institution pathologists at the time of diagnosis. A second retrospective review of the cases was performed by an experienced pathologist (Y.J. with 21 years of experience in liver pathology). A histological diagnosis of cHCC-CC was considered according to the WHO classification 2010, when cells showing features of HCC and CC were present in the same tumor with a combination of HE staining findings and final proof of both hepatocellular and biliary differentiation by immunohistochemical markers [2]. Liver fibrosis was staged according to a METAVIR-equivalent score from F0 to F4: F0, no fibrosis; F1, portal fibrosis without septa; F2, portal fibrosis and few septa; F3, numerous septa without cirrhosis; and F4, cirrhosis [16]. The patients were further classified into three groups: patients with neither liver fibrosis nor cirrhosis (F0, group 1), fibrosis without cirrhosis (F1–3, group 2), and cirrhosis (F4, group 3).

Statistical analysis

All statistical analyses were performed using SPSS 20.0 (Chicago, IL, USA). Continuous variables were compared with the Kruskal–Wallis test. Categorical variables were compared using Fisher's exact test. The mean ADC values of the lesion and liver parenchyma were compared using a paired t test. Interobserver agreements regarding the categorical variables were evaluated using κ statistics. The agreement was rated on the following scale: $\kappa = 0$–0.20, slight agreement; 0.21–0.40, fair agreement; 0.41–0.60, moderate agreement; 0.61–0.80, substantial agreement; and 0.81 or greater, excellent agreement [17]. In cases of disagreement, a third observer (R.F.S.) was asked for an opinion, and a majority decision was reached and used for data analysis. All tests were two sided and $P < 0.05$ was considered statistically significant.

Results

Patient characteristics

The final study group comprised 64 patients with 67 cHCC-CCs. There were 12, 19, and 33 patients in groups 1, 2, and 3, respectively. Evidence of hepatic B viral infection was identified in 58 patients. AFP and CA19-9 levels were elevated in 35 and 14 patients, respectively, and both markers increased in 8 of them. The majority of patients were symptomless ($n = 42$) at the time of initial

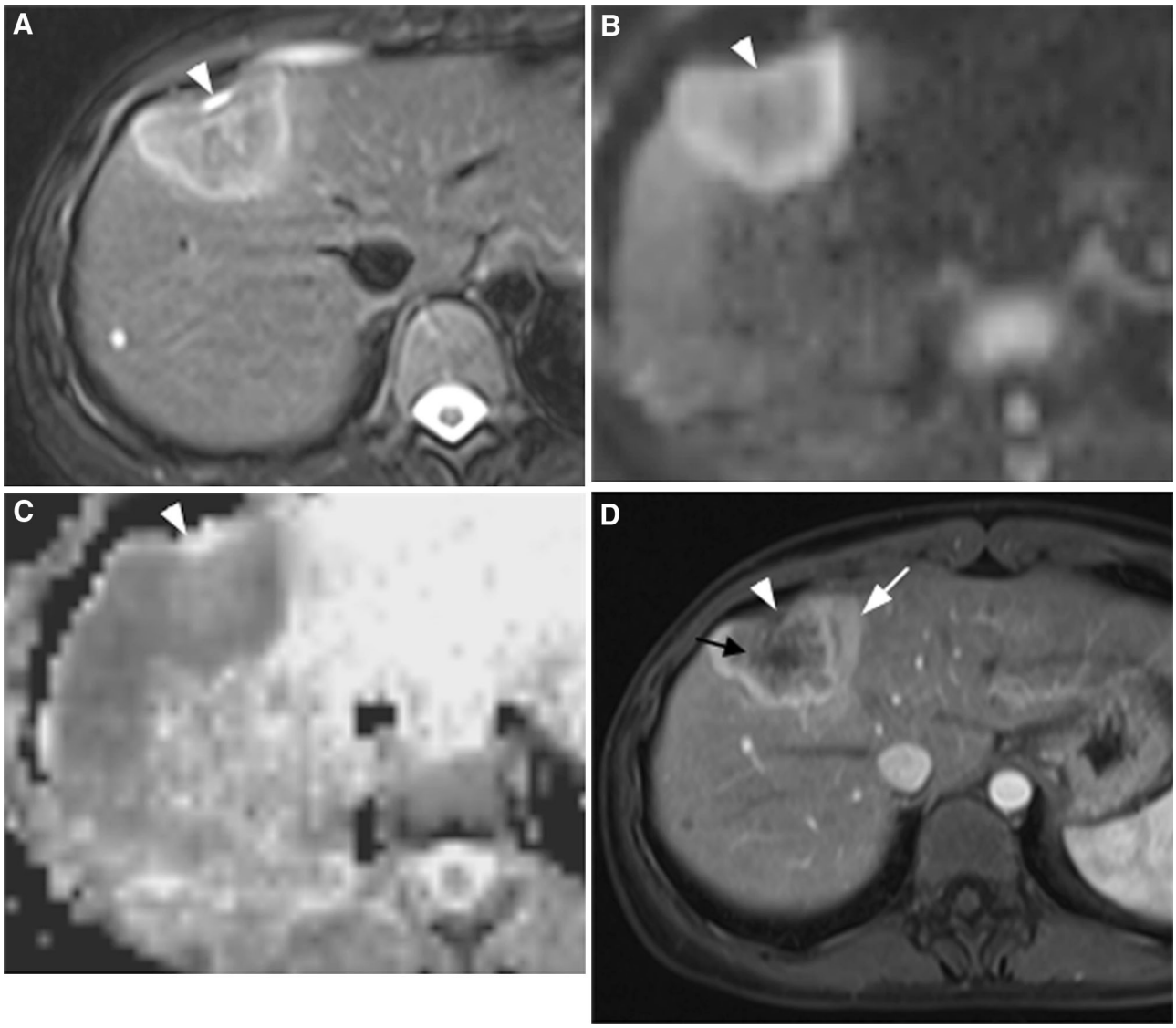

Fig. 2. Combined hepatocellular-cholangiocarcinoma in a 34-year-old woman with fibrosis (F3). **A** Transverse T2-weighted image shows a peripherally hyperintense tumor. **B** Diffusion-weighted image shows peripheral hyperintensity and **C** ADC map shows peripheral hypointensity of the lesion. Transverse T1-weighted VIBE images show **D** peripheral hyperintensity on arterial phase and **E**, **F** a CC-like centripetally progressive enhancement pattern on portal and delayed phases. Note the accompanying mosaic architecture (*black arrow*), transient hepatic intensity difference (*white arrow*), and hepatic capsule retraction (*white arrowheads*). Microscopy shows **G** tumors cells arranged in a tubular, cord-like pattern with marked fibrous stroma (hematoxylin–eosin stain, ×100) and **H** the relatively dense tumor cords in the periphery continuous with the nontumoral liver-cell cords in a replacing growth pattern (*black arrowheads*) (hematoxylin–eosin stain, ×50). **I** Immunohistochemical staining (×100) shows positive EpCAM with stem-cell feature.

medical evaluation, and the most common complaint was abdominal discomfort ($n = 14$). Asymptomatic and symptomatic cases by normal, fibrosis, and cirrhosis were 7, 12, 23 and 5, 7, 10, respectively.

MRI findings

Morphological characteristics

Tumors in the fibrotic (mean size 4.58 cm; interquartile range 3.10–6.38 cm) and cirrhotic livers (mean size 3.70 cm; interquartile range 2.10–4.55 cm) were smaller than those in the normal liver (mean size 5.51 cm; interquartile range 3.05–7.70 cm), and tumors with cirrhosis had the smallest size ($P = 0.0326$). Other morphological features including the nodule number ($P = 0.878$), contour ($P = 0.849$), location ($P = 0.760$), and distribution ($P = 1.000$ and 0.369) were not different among groups.

MR signal characteristics

The categories of T2 signal intensity did not significantly differ between groups ($P = 0.496$), but iso- or hy-

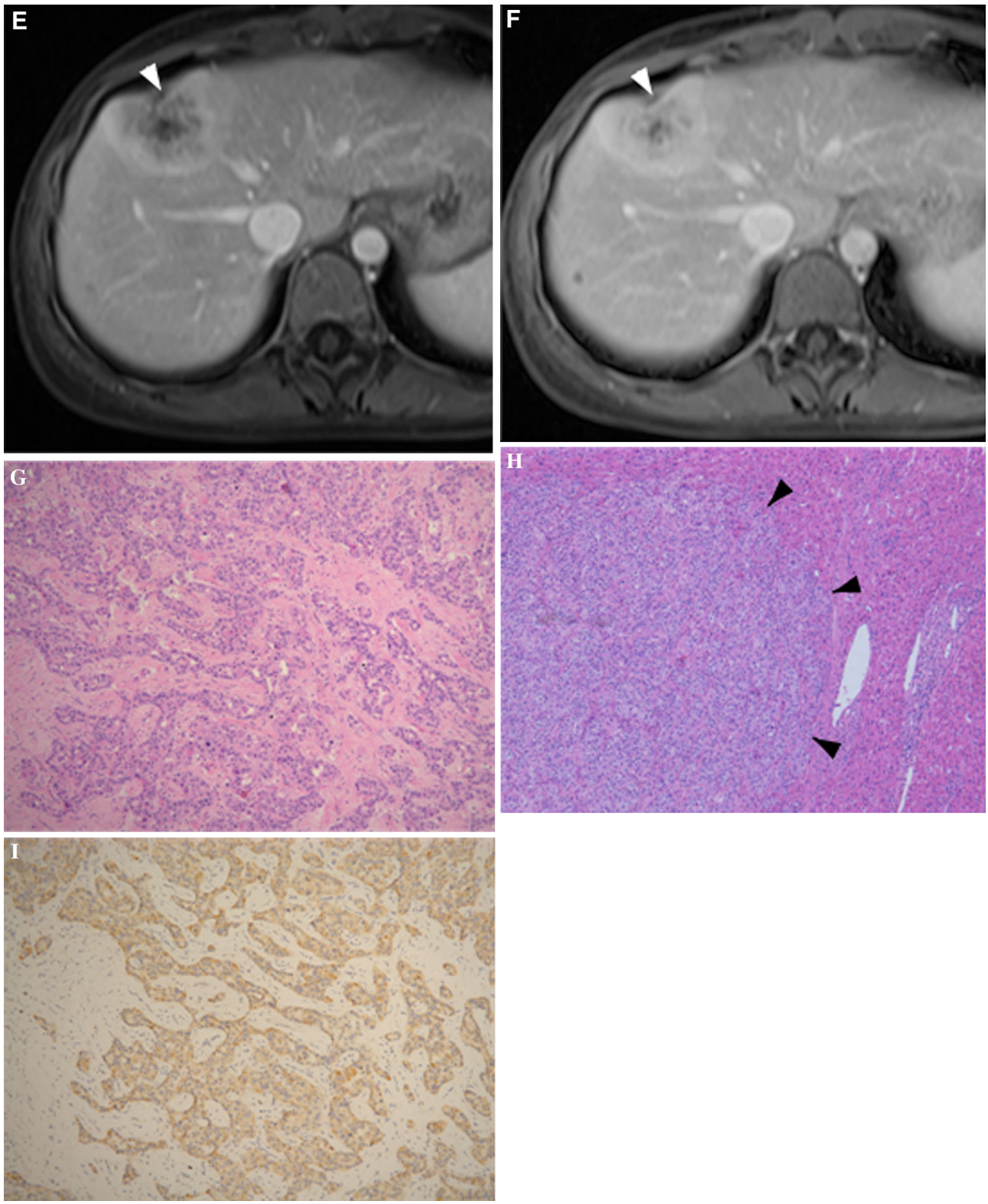

Fig. 2. continued.

pointense lesions were only found in the fibrosis ($n = 2$) or cirrhosis group ($n = 2$, Fig. 1A) (Table 1).

A majority of lesions were heterogeneously ($n = 42$) or peripherally hyperintense ($n = 15$, Fig. 2D) on arterial phase, although no differences were found between groups ($P = 0.191$). During dynamic contrast-enhanced scanning, tumors can be displayed variably, including the CC-like ($n = 30$, Fig. 2), HCC-like ($n = 18$, Fig. 3), and

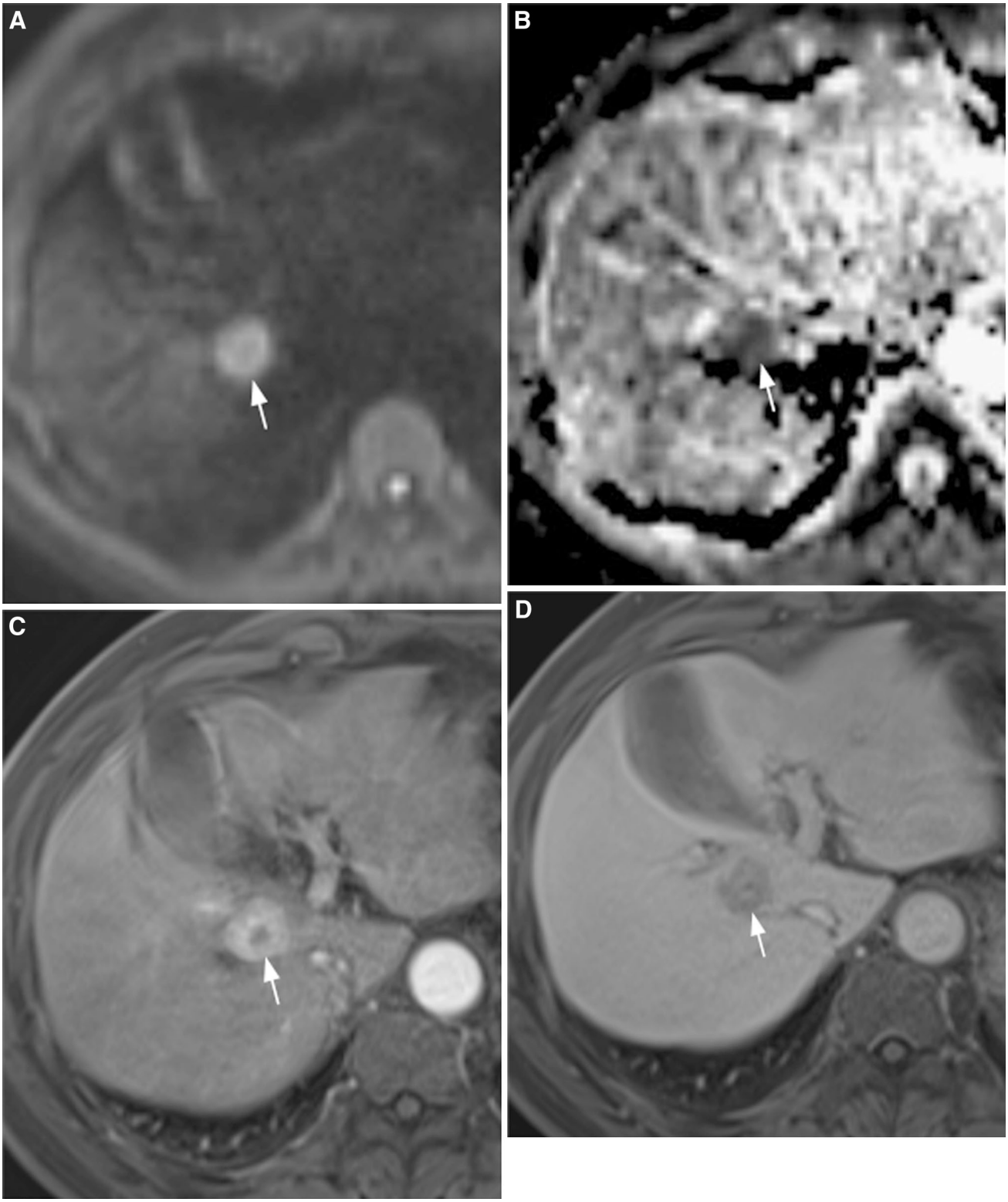

Fig. 3. Combined hepatocellular-cholangiocarcinoma in a 57-year-old man with cirrhosis (F4). **A** Diffusion-weighted image shows marked hyperintensity and **B** ADC map shows marked hypointensity of the lesion. Transverse T1-weighted VIBE images show a HCC-like pattern with **C** contrast uptake on arterial phase, followed by **D** contrast washout with relative hypointensity on delayed phase (*white arrows*).

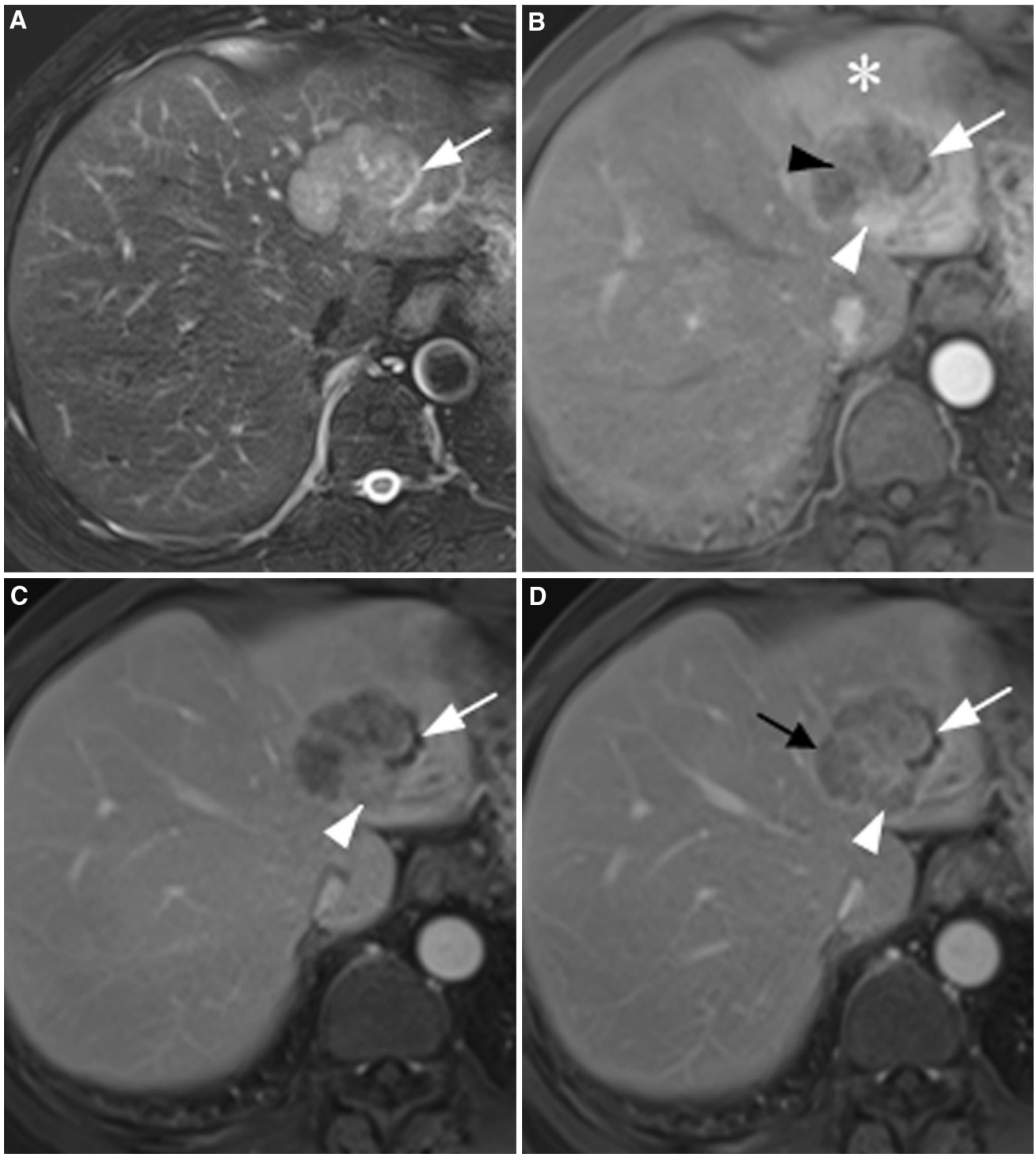

Fig. 4. Combined hepatocellular-cholangiocarcinoma in a 61-year-old man with no fibrosis (F0). **A** Transverse T2-weighted image shows a heterogeneously hyperintense tumor. Transverse T1-weighted VIBE images show a mixed enhancement pattern with **B** predominantly heterogeneous hyperintensity on arterial phase with **C**, **D** a progressive pattern on portal and delayed phases, and the concurrent nodular global hyperintensity on arterial phase with a washout pattern on portal and delayed phases (*white arrowheads*). Note the accompanying delayed capsule-like enhancement (*black arrow*), mosaic architecture (*black arrowhead*), bile duct dilation (*white arrows*), and transient hepatic intensity difference (*white asterisk*). Microscopy shows **E** a border zone between the CC component with abundant fibrous stroma and the HCC component (*black asterisk*) (hematoxylin–eosin stain, ×50) and **F** a clear boundary with incomplete fibrous capsule (*black arrowheads*) and abundant fibrous septations of the tumor (*black arrows* in **E** and **F**) (hematoxylin–eosin stain, ×25).

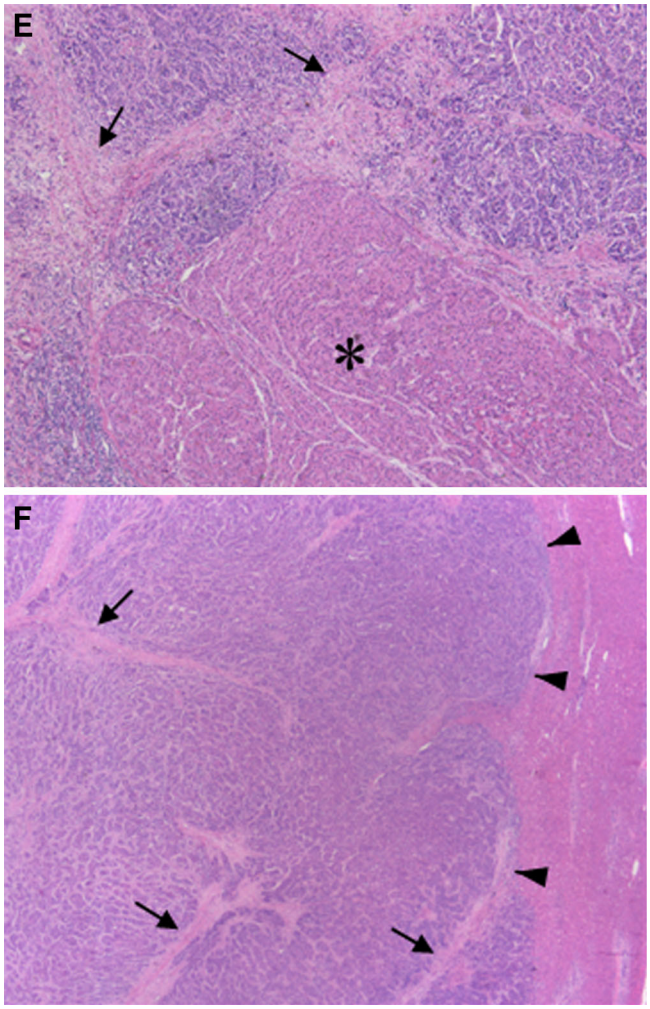

Fig. 4. continued.

mixed (n = 16, Fig. 4) patterns; the manifestations were related to the liver background, as the washout pattern was more often seen in the cirrhosis group when comparing with the noncirrhosis group (P = 0.049). In addition, 3 nodules showed persistently global hyperenhancement after contrast, and they were all small nodules less than 2 cm (Fig. 5; Table 1).

As for the accompanying imaging findings, mosaic architecture (Figs. 2D, 4B) was more commonly seen in the cirrhosis group (P = 0.048). No differences were found with regard to other findings including satellite nodules (P = 0.076), delayed capsule-like enhancement (P = 0.425, Fig. 4D), hepatic capsule retraction (P = 0.374, Fig. 2), hepatic capsule bulging (P = 1.000, Fig. 1), bile duct dilation (P = 0.418, Figs. 1A, 4A–D), THID (P = 0.892, Figs. 2D, 4B), necrosis (P = 0.082), hemorrhage (P = 0.431), vascular invasion (P = 0.393), cancer embolus (P = 1.000, Fig. 6), bile duct invasion (P = 0.695, Fig. 1E, F), positive lymph node (P = 1.000), and distant metastasis (P = 0.739) (Table 1).

On DWI, all lesions were hyperintense to varying degrees (Figs. 2B, 3A), and the mean ADC value of the lesions was significantly lower than that of the surrounding liver (Figs. 2C, 3B) (t = 6.464, $P < 0.001$); but the absolute ADC values of the lesions were not different among the three groups (P = 0.899) (Table 1).

Good agreement between the two observers was obtained for all measured categorical parameters (κ = 0.811–0.980).

Discussion

In our study, cHCC-CC was male predominant in the middle 50s with high hepatitis B viral infection rate and elevated AFP level, more like HCC, consistent with previous studies [6, 9, 11]. Overall, tumors in the fibrotic and cirrhotic livers were smaller than those in the normal liver, which may be corresponded to a more frequent follow-up in these patients, thus regular surveillance may be necessary.

Related to the spectrum of pathologic findings, cHCC-CC has imaging appearances overlapping with both HCC and CC. Our study showed that despite the similarities between cHCC-CC and HCC in clinical features, it may resemble CC more closely in the enhancement pattern (the CC-like centripetally progressive or persistent pattern) overall, similar to many prior studies [5, 13, 18]. Thus, discordance between enhancement pattern and clinical features suggests the possibility of cHCC-CC to a certain extent. Meanwhile, a mixed manifestation of both tumors was not rarely seen, which is also characteristic and highly suggests cHCC-CC. Notably, the HCC-like enhancement pattern displayed with higher percentage in cirrhosis background when comparing with that in noncirrhosis background, partly concurring with de Campos et al. [14] who indicated that early enhancement with partial washout on later phases seemed to be the more common enhancement pattern in cirrhotic livers. This may be related to the susceptibility of HCC generation in this specific background and would increase difficulties in differential diagnosis. But further studies are needed to validate our data and achieve more convincing conclusions. In addition, 3 lesions showed atypical persistently global hyperenhancement after contrast, and this may be corresponded to their small nodule size less than 2 cm with relatively high perfusion. It is also worth noting that confusing feature of iso/hypointensity on T2WI was exclusively found in the fibrosis and cirrhosis groups, and this may be explained by the distortion of the hepatic parenchyma due to the fibrotic process and the particular profile caused by portal hypertension and associated circulatory disturbances [19, 20].

Apart from the imaging features above, analysis combined with other accompanying findings is necessary. In our cases, accompanying delayed capsule-like enhancement, mosaic architecture, bile duct dilation, THID, and necrosis occurred frequently, but none of

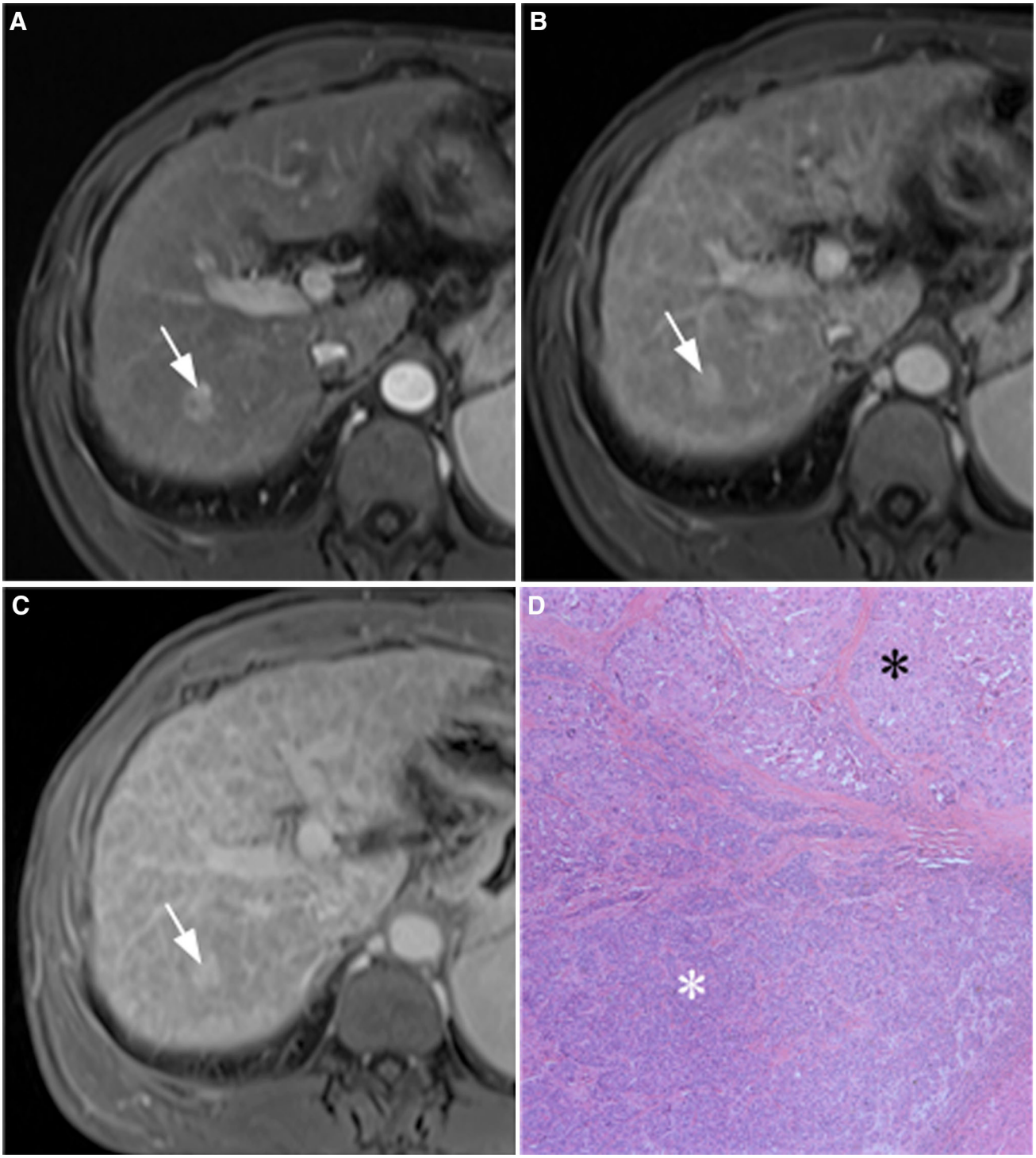

Fig. 5. Combined hepatocellular-cholangiocarcinoma in a 45-year-old man with cirrhosis (F4). Transverse T1-weighted VIBE images show **A** global hyperintensity on arterial phase and (**B**, **C**) a persistently global hyperenhancement pattern on portal and delayed phases (*white arrows*). **D** Microscopy shows a border zone between the CC component (*white asterisk*) and the HCC component (*black asterisk*) with dense cellularity (hematoxylin–eosin stain, ×50).

these findings are sensitive or specific for cHCC-CC. Nevertheless, our study revealed that mosaic architecture presented more in the cirrhosis background. Potretzke et al. [10] indicated mosaic architecture as an ancillary feature favoring malignancy and HCC specifically, and the concurring more commonly seen mosaic architecture and HCC-like enhancement pattern in cirrhosis background of our study coincided with the theory to a cer-

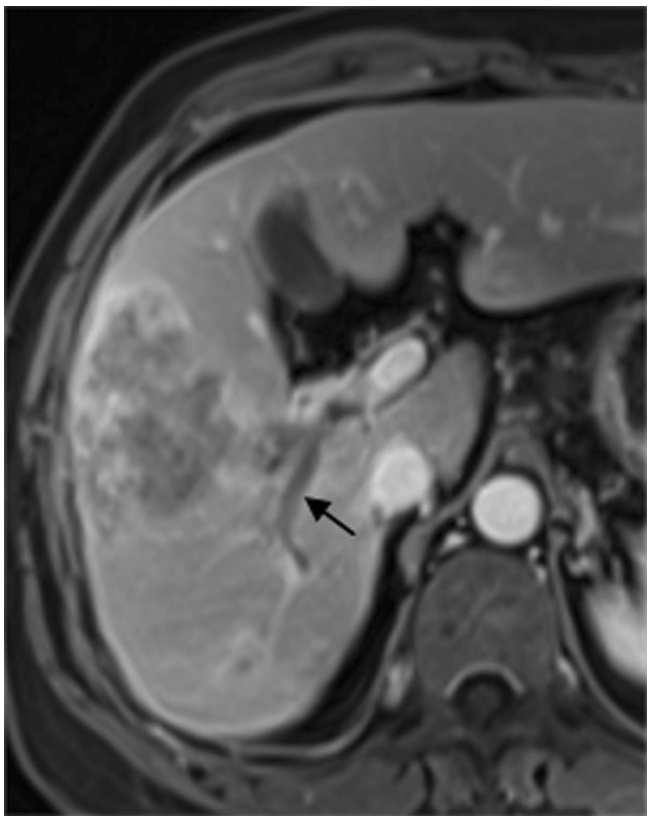

Fig. 6. Combined hepatocellular-cholangiocarcinoma in a 58-year-old man with mild fibrosis (F1). Note the cancer embolus in the right branch of portal vein (*black arrow*).

tain extent. This may be explained by the abundant fibrous stroma and segregation histopathologically which may be partly related to the disturbed blood supply and the distortion of the hepatic parenchyma under cirrhotic background.

DWI is an increasingly used MR technique, which enables the visualization of diffusivity of water molecules, and may provide information regarding the cellular density and properties of the extracellular matrix [21]. All lesions were hyperintense on DWI, and the marked restricted diffusion can raise suspicion for cHCC-CC, which was supported by Potretzke et al. [10]. However, DWI is hampered by the low specificity, and there are substantial overlaps in the range of ADCs among cHCC-CC in normal, fibrotic, and cirrhotic livers. Overall, while restricted diffusion may not significantly differ between different liver backgrounds, careful evaluation of ADC may be helpful for including cHCC-CC in differential diagnosis.

This study had several limitations. First, our study was a retrospective research, thus only one time point was assessed, and selection bias may exist; further prospective studies would be necessary. Second, thorough analysis of different stages of liver fibrosis was not performed. Third, our study mainly discussed the key points of differentiating the MR features of cHCC-CC in normal, fibrotic, and cirrhotic livers, and direct comparison with pure HCC and CC was not performed in detail. Finally, we used traditional extracellular contrast agent (gadopentetate dimeglumine). Nowadays, liver-specific contrast agents (e.g., gadoxetic acid) are increasingly used for detection and characterization of focal liver lesion, and further studies are needed to confirm their potential advantages in the differentiation of cHCC-CC. Despite these limitations, our study included a relatively large study population and provided valuable information for the diagnosis and differential diagnosis of cHCC-CC in normal, fibrotic, and cirrhotic livers.

In conclusion, the nodule size, enhancement pattern, and the presence of mosaic architecture in cHCC-CC differ between normal, fibrotic, and cirrhotic livers. cHCC-CC in cirrhotic liver is more likely to present as a small tumor with washout pattern and mosaic architecture. Given the frequently confusing imaging appearances and the discordance between clinical features and imaging findings, biopsy would be necessary in particular cases.

Acknowledgments. This study was funded by the National Natural Science Foundation of China (Grant Number 81571661), the Shanghai Sailing Program (Grant Number 16YF1410600), and the Youth Science Foundation of Zhongshan Hospital, Fudan University (Grant Number 2015ZSQN14).

Compliance with ethical standards

Conflict of interest Ruo Fan Sheng, Yan Hong Xie, Yuan Ji, Cai Zhong Chen, Li Yang, Kai Pu Jin, and Meng Su Zeng declare that they have no conflict of interest.

Ethical approval All procedures performed in studies involving human participants were in accordance with the ethical standards of the institutional and/or national research committee and with the 1964 Helsinki declaration and its later amendments or comparable ethical standards.

Informed consent This retrospective study was approved by the institutional review board and informed consent was waived.

References

1. O'Connor K, Walsh JC, Schaeffer DF (2014) Combined hepatocellular-cholangiocarcinoma (cHCC-CC): a distinct entity. Ann Hepatol 13:317–322
2. Yeh MM (2010) Pathology of combined hepatocellular-cholangiocarcinoma. J Gastroenterol Hepatol 25:1485–1492
3. Park H, Choi KH, Choi S-B, et al. (2011) Clinicopathological characteristics in combined hepatocellular-cholangiocarcinoma: a single center study in Korea. Yonsei Med J 52:753–760
4. Kim SH, Park YN, Lim JH, et al. (2014) Characteristics of combined hepatocellular-cholangiocarcinoma and comparison with intrahepatic cholangiocarcinoma. Eur J Surg Oncol 40:976–981
5. Shetty AS, Fowler KJ, Brunt EM, et al. (2014) Combined hepatocellular-cholangiocarcinoma: what the radiologist needs to know about biphenotypic liver carcinoma. Abdom Imaging 39:310–322
6. Yin X, Zhang B-H, Qiu S-J, et al. (2012) Combined hepatocellular carcinoma and cholangiocarcinoma: clinical features, treatment modalities, and prognosis. Ann Surg Oncol 19:2869–2876

7. Garancini M, Goffredo P, Pagni F, et al. (2014) Combined hepatocellular-cholangiocarcinoma: a population-level analysis of an uncommon primary liver tumor. Liver Transplant 20:952–959
8. Ikeda H, Harada K, Sato Y, et al. (2013) Clinicopathologic significance of combined hepatocellular-cholangiocarcinoma with stem cell subtype components with reference to the expression of putative stem cell markers. Am J Clin Pathol 140:329–340
9. Lee SD, Park S-J, Han S-S, et al. (2014) Clinicopathological features and prognosis of combined hepatocellular carcinoma and cholangiocarcinoma after surgery. Hepatobiliary Pancreat Dis Int 13:594–601
10. Potretzke TA, Tan BR, Doyle MB, et al. (2016) Imaging features of biphenotypic primary liver carcinoma (hepatocholangiocarcinoma) and the potential to mimic hepatocellular carcinoma: LI-RADS analysis of CT and MRI features in 81 cases. AJR Am J Roentgenol 11:1–7
11. Chu K-j Lu, C-d Dong H, X-h Fu, H-w Zhang, X-p Yao (2014) Hepatitis B virus-related combined hepatocellular-cholangiocarcinoma: clinicopathological and prognostic analysis of 390 cases. Eur J Gastroenterol Hepatol 26:192–199
12. Razumilava N, Gores GJ (2014) Liver transplantation for intrahepatic cholangiocarcinoma—Authors' reply. Lancet 384:1182–1183
13. Wells ML, Venkatesh SK, Chandan VS, et al. (2015) Biphenotypic hepatic tumors: imaging findings and review of literature. Abdom Imaging 40:2293–2305
14. de Campos ROP, Semelka RC, Azevedo RM, et al. (2012) Combined hepatocellular carcinoma-cholangiocarcinoma: report of MR appearance in eleven patients. J Magn Reson Imaging 36:1139–1147
15. Truant S, Boleslawski E, Duhamel A, et al. (2012) Tumor size of hepatocellular carcinoma in noncirrhotic liver: a controversial predictive factor for outcome after resection. Eur J Surg Oncol 38:1189–1196
16. Bedossa P, Poynard T (1996) An algorithm for the grading of activity in chronic hepatitis C. Hepatology 24:289–293
17. Landis JR, Koch GG (1977) Measurement of observer agreement for categorical data. Biometrics 33:159–174
18. Fowler KJ, Sheybani A, Parker RA III, et al. (2013) Combined hepatocellular and cholangiocarcinoma (biphenotypic) tumors: imaging features and diagnostic accuracy of contrast-enhanced CT and MRI. AJR Am J Roentgenol 201:332–339
19. Rimola J, Forner A, Reig M, et al. (2009) Cholangiocarcinoma in cirrhosis: absence of contrast washout in delayed phases by magnetic resonance imaging avoids misdiagnosis of hepatocellular carcinoma. Hepatology 50:791–798
20. Gupta AA, Kim DC, Krinsky GA, Lee VS (2004) CT and MRI of cirrhosis and its mimics. AJR Am J Roentgenol 183:1595–1601
21. Schelhorn J, Best J, Reinboldt MP, et al. (2015) Does diffusion-weighted imaging improve therapy response evaluation in patients with hepatocellular carcinoma after radioembolization? Comparison of MRI using Gd-EOB-DTPA with and without DWI. J Magn Reson Imaging 42:818–827